AGU ADVANCING EARTH AND SPACE SCIENCE

Geophysical Research Letters

RESEARCH LETTER
10.1029/2021GL092779

Estimating Dissipation Rates Associated With Double Diffusion

L. Middleton[1,2], E. C. Fine[3], J. A. MacKinnon[4], M. H. Alford[4], and J. R. Taylor[1]

[1]Department of Applied Mathematics and Theoretical Physics, University of Cambridge, Centre for Mathematical Sciences, Cambridge, UK, [2]British Antarctic Survey, Cambridge, UK, [3]Woods Hole Oceanographic Institution, Falmouth, MA, USA, [4]Scripps Institution of Oceanography, La Jolla, CA, USA

Key Points:

- We develop a method for estimating dissipation rates due to double-diffusive convection from temperature and salinity data using an energetic argument
- The method reproduces the patterns and magnitude of dissipation rates and heat fluxes from microstructure measurements across an arctic eddy
- The technique performs well even when applied to lower resolution Conductivity, Temperature, Depth (CTD) data

Correspondence to:
L. Middleton,
lm758@cam.ac.uk

Citation:
Middleton, L., Fine, E. C., MacKinnon, J. A., Alford, M. H., & Taylor, J. R. (2021). Estimating dissipation rates associated with double diffusion. *Geophysical Research Letters*, *48*, e2021GL092779. https://doi.org/10.1029/2021GL092779

Received 31 JAN 2021
Accepted 17 JUN 2021

Abstract Double diffusion refers to a variety of turbulent processes in which potential energy is released into kinetic energy, made possible in the ocean by the difference in molecular diffusivities between salinity and temperature. Here, we present a new method for estimating the kinetic energy dissipation rates forced by double-diffusive convection using temperature and salinity data alone. The method estimates the up-gradient diapycnal buoyancy flux associated with double diffusion, which is hypothesized to balance the dissipation rate. To calculate the temperature and salinity gradients on small scales we apply a canonical scaling for compensated thermohaline variance (or 'spice') on sub-measurement scales with a fixed buoyancy gradient. Our predicted dissipation rates compare favorably with microstructure measurements collected in the Chukchi Sea. Fine et al. (2018), https://doi.org/10.1175/jpo-d-18-0028.1, showed that dissipation rates provide good estimates for heat fluxes in this region. Finally, we show the method maintains predictive skill when applied to a sub-sampling of the Conductivity, Temperature, Depth (CTD) data.

Plain Language Summary Understanding the transport of heat in the Arctic Ocean is vital for predicting the fate of sea-ice in the decades to come. Small-scale turbulence is an important driver of heat transport and one of the major forms of this turbulence is known as 'double-diffusive convection'. This is where gradients in temperature and salinity drive turbulence. It is only possible because salinity diffuses significantly slower than temperature, hence the name 'double-diffusive'. The most direct measurements of ocean mixing require sampling velocity or temperature gradients on scales <1 mm, so-called microstructure measurements. Here we present a new method for estimating the energy dissipated by double-diffusive convection using temperature and salinity measurements on larger scales (100s–1000s of metres). We apply the method to a high-resolution survey of temperature and salinity through a subsurface Arctic eddy and compare the results with simultaneous microstructure measurements. The new technique can reproduce up to 72% of the observed dissipation rates to within the measurement uncertainty. This suggests the method could be used to estimate the dissipation and so heat fluxes associated with double-diffusive convection in regions without microstructure measurements. The method also performs well when applied to data sub-sampled on larger scales.

1. Introduction

Recent decades have seen a decline in Arctic sea-ice thickness and extent (E. Carmack et al., 2015). Sea-ice melting is influenced by vertical ocean heat transport (Timmermans & Marshall, 2020). For example, a doubling of the Beaufort Gyre halocline heat content has influenced sea-ice extent (Shimada et al., 2006; Timmermans et al., 2018). Heat exchange between the surface layer and sub-surface water masses depends on small-scale turbulent processes and identifying turbulent regions helps to quantify this heat flux (Fine et al., 2018). The most direct measurements of turbulent mixing require high-resolution measurements (microstructure) which are costly and difficult to obtain across large spatial scales. A natural solution is to parameterize turbulence based on properties measured on the finescale (e.g., Polzin et al., 2014; Whalen et al., 2015). However, common shear and strain based parameterisations for internal wave breaking do not apply well to areas of double-diffusive convection (Gregg, 1989).

Buoyancy gradients in the upper Arctic Ocean are dominated by salinity, which enables heat to be trapped sub-surface. Opposing vertical gradients in temperature (T) and salinity (S) and a relatively weak internal

wave field make the Arctic favorable for double-diffusive convection (e.g., Bebieva & Timmermans, 2016), where it can play a dominant role in upwards transport of the trapped heat (E. C. Carmack et al., 2012). Double-diffusive convection refers to convective processes that rely on the difference between the molecular diffusivities of heat ($\kappa_T \sim \mathcal{O}(10^{-7})\ \mathrm{m^2 s^{-1}}$) and salt ($\kappa_S \sim \mathcal{O}(10^{-10})\ \mathrm{m^2 s^{-1}}$) (Schmitt, 1994). A variety of flow structures may develop due to double diffusion. For example, vertical gradients in temperature and salinity can force convective motions, leading to step-like temperature and salinity profiles in a thermohaline 'staircase' (e.g., Timmermans et al., 2008). Other results of double diffusion include thermohaline intrusions (Ruddick & Kerr, 2003; Ruddick & Richards, 2003) and salt fingers (Kunze, 2003). Traditionally these processes are analyzed and parameterized separately, however, recently Middleton and Taylor (2020) presented an energetic framework that describes the dynamics of all cases where potential energy is released into kinetic energy via double diffusion (our definition of double-diffusive convection).

Several studies have shown a close connection between large-scale circulation and double-diffusive fluxes. Shibley et al. (2017) showed that the prevalence of thermohaline staircases, and by inference the double-diffusive fluxes, are modified by the large-scale circulation patterns within the Arctic basins. Individual layers associated with thermohaline staircases can extend for several hundred kilometers with significant variations in T/S properties along this length (Bebieva & Timmermans, 2019). This suggests a possible connection between lateral fluxes of heat and salt and vertical fluxes associated with double-diffusive convection.

Estimating double-diffusive heat fluxes generally requires either microstructure measurements or parameterizations of specific double-diffusive processes. For example, Shibley et al. (2017) use a 4/3 flux law to estimate heat fluxes across diffusive interfaces in thermohaline staircases, and Inoue et al. (2007) combine two parameterisations for different double-diffusive regimes, distinguished using the density ratio $R_\rho = \alpha \frac{\partial T}{\partial z} \Big/ \beta \frac{\partial S}{\partial z}$. Fine et al. (2018) showed that the turbulent dissipation rate can be used to infer the vertical heat flux in double-diffusive conditions. Here, we propose a new statistical technique to estimate turbulent dissipation rates associated with general double-diffusive processes from a Conductivity, Temperature, Depth (CTD) section. We rely on the notion that lateral stirring of T/S along isopycnals (surfaces of constant density) gives rise to large T/S gradients that are 'compensated' in terms of their contribution to density (Rudnick & Ferrari, 1999). This compensated T/S (or 'spice') variance is preferentially fluxed to small scales.

The central concept behind our method is that large spice gradients generated by along-isopycnal stirring drive double-diffusive motions through an up-gradient buoyancy flux and that the resulting small-scale turbulence fluxes energy further down scale until it is ultimately dissipated. We use a synthetic model spectrum to extrapolate along-isopycnal spice variance measured from a CTD section down to the scale of the largest turbulent overturns and use this result along with other assumptions to estimate the up-gradient buoyancy flux and the turbulent dissipation rate through the framework described in Middleton and Taylor (2020).

The standard model for shear-driven ocean mixing is that energy is input to small scales via shear forced by a larger structure (e.g., internal waves and mean flows). Some portion of this energy gets transferred to micro-scales and ultimately dissipated at a rate ϵ, and some portion is lost to potential energy via the turbulent buoyancy flux $w'b'$; used to irreversibly mix the density field. This division is quantified using a parameter Γ, the flux coefficient (Gregg et al., 2018), that has been evaluated from observations, experiments and simulations (e.g., Holleman et al., 2016; Howland et al., 2020; Jackson & Rehmann, 2003). The complication is that the exchange of potential energy and kinetic energy via $w'b'$ is reversible and in fact dominated by adiabatic internal waves. This was resolved by Winters et al. (1995) who divided the potential energy into a 'Background Potential Energy' (BPE) and an 'Available Potential Energy' (APE) and considered their budgets. They found that APE is transformed into BPE via a diapycnal (across surfaces of constant density) buoyancy flux ϕ_d, which they associated with 'irreversible mixing' of density as ϕ_d is always positive in a single-component fluid. However, in double-diffusive convection, variations in density (i.e., APE) are created by the action of diffusion, so the standard model of shear-driven irreversible mixing of density does not apply.

Extending the Winters et al. (1995) framework to include double diffusion, Middleton and Taylor (2020) showed that the 'mixing' of density may be reversed; in a double-diffusive fluid, BPE (as defined in Winters et al., 1995) can be converted into APE via an up-gradient diapycnal buoyancy flux, i.e., $\phi_d < 0$. In a

statistically steady state, we might then expect the generation of APE to be converted into kinetic energy through the vertical turbulent buoyancy flux, i.e., $\langle w'b' \rangle \simeq -\langle \phi_d \rangle$, averaging across an appropriate volume. Further, if double-diffusive convection is the only source of turbulence, then the input of kinetic energy comes entirely from potential energy, so the average rate of dissipation of kinetic energy, $\langle \epsilon \rangle$, should balance the vertical turbulent buoyancy flux $\langle w'b' \rangle$, which gives the balance $\langle \epsilon \rangle \simeq \langle w'b' \rangle \simeq -\langle \phi_d \rangle$. The form for ϕ_d can be expressed in terms of the local gradients in temperature and salinity and their respective molecular diffusivities, which provides a pathway for predicting the dissipation rate associated with double diffusion from T and S alone.

The diapycnal buoyancy flux, ϕ_d, as formulated by Middleton and Taylor (2020), involves the *molecular* diffusive fluxes of heat and salt. Therefore, diagnosing ϕ_d requires three-dimensional gradients of T and S at small scales. While this is possible in direct numerical simulations, it is not practical using observational data. Here, we follow the theory of Haynes and Anglade (1997) and Smith and Ferrari (2009) and assume that spice is stirred along isopycnals by quasi-geostrophic motions. The possibility of double-diffusive instabilities developing in response to along-isopycnal stirring of spice was raised in Garrett (1982) and Smith and Ferrari (2009). However, we believe this letter is the first attempt to use this principle to estimate the dissipation rate associated with double-diffusive processes.

To demonstrate our method and test the underlying assumptions, we use a CTD section through a sub-surface warm-core eddy reported in Fine et al. (2018) and compare our estimated dissipation rates with those inferred from microstructure measurements. Fine et al. (2018) surveyed an intrahalocline warm-core eddy on the Chuchki Slope in September 2015, collecting shear and thermal microstructure data as well as finescale T and S across multiple eddy transects. Eddies such as this are thought to be an important source of heat into Canada Basin (Watanabe, 2011), where the implications for sea-ice are not well understood. This was confirmed by Fine et al. (2018), who showed that the regions of enhanced heat flux at the top of the eddy, inferred from thermal microstructure data, could lead to a significant upwards heat flux if extrapolated over the eddy's lifetime. Fine et al. (2018) found that the top of the eddy was also associated with enhanced dissipation rates, which were used to estimate the heat flux.

The method we introduce in this letter uses physical reasoning to link along-isopycnal stirring of spice with double-diffusive convection and ultimately energy dissipation. The primary assumption that we make is that double-diffusive convection is the sole driver of turbulence i.e., shear production is negligible. This is analogous to the assumption made in finescale internal wave parameterisations that shear production from internal waves is the sole driver of turbulence (e.g. Polzin et al., 2014). When compared with the data from Fine et al. (2018), the dissipation rate inferred using our method closely matches the dissipation rate inferred from a microstructure probe except in regions with relatively low Richardson number where Fine et al. (2018) hypothesized that shear-driven turbulence was active. This shows that our method can be used in conjunction with more direct microstructure measurements to identify the relative importance of double diffusion. When microstructure measurements are not available, our method provides a means to estimate the turbulent dissipation rate in regions that are dominated by double diffusion from a high resolution CTD section.

This letter is organized as follows. In the first section we introduce the observations from Fine et al. (2018). In the second section we describe the method for estimating turbulent dissipation rates associated with double-diffusive convection. In the third section we compare our results to the observations. We find a good match across most of the section, including the top of the eddy, where dissipation rates can be linked to the vertical heat flux. We also find a good match across 'doubly-stable' regions without opposing background T/S gradients. The estimated double-diffusive dissipation rate is significantly smaller than the microstructure dissipation rate only in regions where the gradient Richardson number is low and the buoyancy Reynolds number $Re_b > 20$, indicating active shear-driven turbulence. Finally, we test how the method performs on a coarse sub-sampling of the data, suggesting applicability to data with lower spatial resolution.

2. Observations

In this section we briefly discuss the observations from the Arctic Ocean that we use to test the new method for estimating the double-diffusive dissipation rate. This data will also be used to test some assumptions made in the next section. Fine et al. (2018) described data collected from an anomalously warm anti-cyclon-

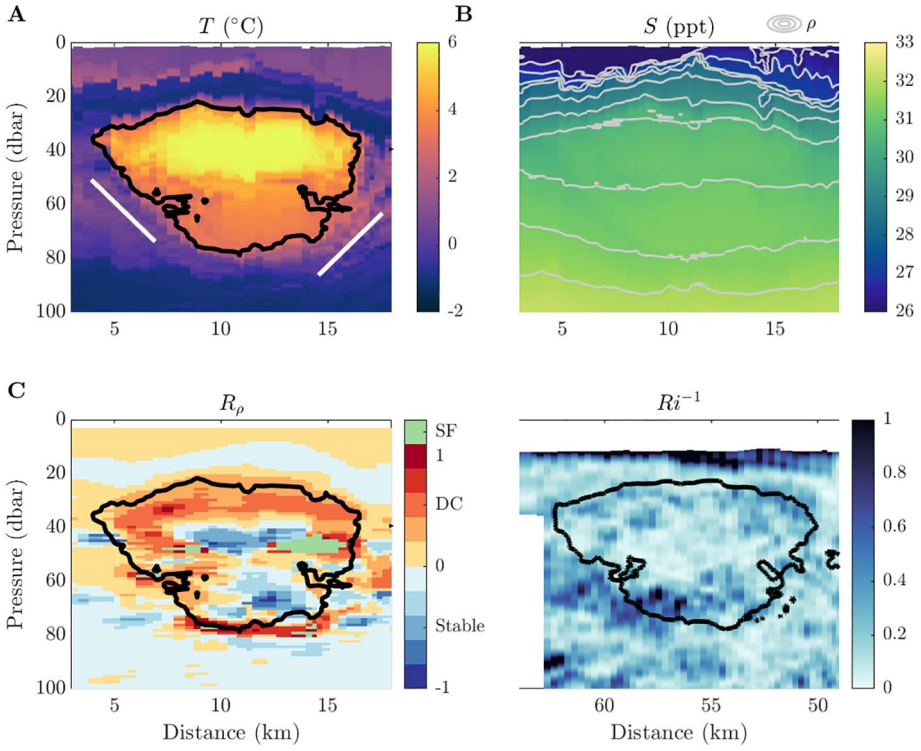

Figure 1. (a) Temperature with 3°C contour in black and angle f/N marked with white lines, with value calculated at line midpoint. (b) Salinity with contours of ρ (kgm^{-3}) in gray. (c) Density ratio $R_\rho = \alpha \frac{\partial T}{\partial z} \Big/ \beta \frac{\partial S}{\partial z}$. (d) Shear $U_z = \sqrt{u_z^2 + v_z^2}$.

ic eddy on the Chukchi slope in September 2015. The temperature and salinity from one of the sections are shown in Figure 1. Isopycnals are shown in gray in panel b and the 3°C isotherm which outlines the eddy is shown in black. In most places density variations are controlled by salinity, although temperature plays a role within the eddy. Concurrent microstructure measurements of the kinetic energy dissipation rate, ϵ, and thermal variance dissipation, χ_T, were used to identify regions of high dissipation along the top, sides and bottom of the eddy. Practical issues regarding the processing of microstructure data in the presence of thermohaline layering and instrument noise floors are discussed in Fine et al. (2018) and not included here. The heat flux was also inferred from the microstructure profiles and used to estimate the lifetime of the eddy. The lateral heat flux along the eddy flanks ($\sim$ 2,000 Wm^{-2}) was found to have the largest impact on the eddy evolution, giving an estimated eddy lifetime of $\sim$1 year, although the heat flux along the top of the eddy (5 Wm^{-2}) was also significant. The dissipation rate, ϵ, was used to estimate the heat flux using the Osborn (1980) model, where a good agreement was found with the estimates from χ_T using the Osborn and Cox (1972) model.

The data from Fine et al. (2018) provides a useful testing grounds for our method since it contains a variety of regimes. Different processes were identified by Fine et al. (2018) based on visual identification of coherent features (layers and intrusions), Richardson number $Ri^{-1} = U_z^2 / N^2$ (see Figure 1) and the relative alignment of temperature and salinity gradients. The density ratio R_ρ (plotted in Figure 1, smoothed with a median filter) indicates a 'Diffusive Convection'-favorable (DC) region along the top of the eddy where staircases were observed ($0 < R_\rho < 1$), a 'Salt-Fingering'-favorable (SF) region in the middle and at the base of the eddy ($R_\rho > 1$) and a 'Doubly-Stable' region within and below the eddy ($R_\rho < 0$) where shear-driven mixing was thought to occur based on the enhanced Richardson number below the eddy (panel d). Traditionally, different types of double-diffusive convection are parameterized separately (e.g., Inoue et al., 2007). However, our method does not depend on the type of double diffusion based on measured T/S gradients, instead assuming that the opposing gradients necessary for double diffusion are created by sub-measurement scale

spice variance. The T/S gradients can take any alignment relative to one another, subject to the condition for an up-gradient diapycnal buoyancy flux (Φ_d) derived in Middleton and Taylor (2020).

3. Method

In this section we start by presenting a new form for the diapycnal buoyancy flux, ϕ_d, in terms of spice gradients before describing our method for down-scaling the observed spice gradients (i.e., inferring their size at sub-measurement scales) in order to estimate ϕ_d and the dissipation rate, ϵ.

Our method can be summarized as follows. First, assuming double-diffusive convection is the driver of turbulence, we take $\langle\epsilon\rangle = -\langle\phi_d\rangle$, where $\langle\cdot\rangle$ is an implicit average over the volume between observations. The diapycnal flux ϕ_d is then re-expressed in terms of spice gradients and buoyancy gradients. We assume that the buoyancy and spice gradients are anti-correlated, justified with reference to the observations, which gives an approximate upper bound for $-\langle\phi_d\rangle$. Hypothesizing that the sub-measurement scales are dominated by quasi-geostrophic (QG) stirring along isopycnals, we assume the buoyancy gradients are constant and the spice variance is modeled with the QG wavenumber scaling for passive tracers i.e., $\tilde{k}^{-1}$ in stretched coordinates. This scaling is taken to hold down to the critical scale at which ϕ_d drives convective overturns. The amplitude of the synthetic spice power spectrum is estimated using a two-point correlation calculated locally from the observations. The power spectrum is then used to estimate the mean spice gradient magnitude down to the overturning scale, which is then used to estimate ϕ_d and ϵ.

3.1. Diapycnal Buoyancy Flux

Middleton and Taylor (2020) wrote the diapycnal buoyancy flux

$$\phi_d = \frac{(g\kappa_T\alpha\nabla T - g\kappa_S\beta\nabla S)\cdot\nabla b}{b_z^*}, \tag{1}$$

where (κ_T, κ_S) are the molecular diffusivities for T and S, g is the gravitational acceleration, $b = g\alpha T - g\beta S$ is the buoyancy using a linear equation of state for (α, β) the coefficients of thermal expansion and haline contraction respectively, and b_z^* is the gradient of the sorted buoyancy profile.

The definition of spice is complicated by the nonlinear equation of state (Jackett & McDougall, 1985). However, we will use a linear approximation and define spice as $s_p \equiv \alpha T + \beta S$. Our method is applied across small changes in temperature (T) and salinity (S) between CTD casts, and so it is reasonable to assume linearity on the sub-measurement scale. We can re-express T and S in terms of buoyancy (b) and spice, i.e., $g\alpha T = (gs_p + b)/2$ and $g\beta S = (gs_p - b)/2$, where g is the gravitational acceleration. This leads to the new expression

$$\phi_d = \frac{\kappa_T + \kappa_S}{2b_z^*}\left|\nabla b\right|^2 + g\frac{\kappa_T - \kappa_S}{2b_z^*}\nabla b\cdot\nabla s_p. \tag{2}$$

In the single-component limit where the two diffusivities are equal, the second term disappears, so we can consider it as a double-diffusive contribution. Using molecular values for the diffusivities, $\kappa_T \gg \kappa_S$ so $\kappa_T + \kappa_S \approx \kappa_T \approx \kappa_T - \kappa_S$ and hence the two prefactors are of similar size, aside from the factor of g.

In order to estimate the dissipation rate due to double diffusion, we will assume that the dissipation is entirely forced by an up-gradient buoyancy flux as discussed in the introduction. Middleton and Taylor (2020) showed that BPE is converted into APE when the average of ϕ_d over a given volume (Φ_d) is negative. Here, we attempt to estimate $\Phi_d \equiv \phi_d$ where angle brackets denote an average over a volume bounded by neighboring T/S measurement points. We then assume that all of the potential energy released by the up-gradient buoyancy flux is converted into kinetic energy and ultimately dissipated and set $\epsilon = -\phi_d$.

The average of Equation 2 involves the correlation between buoyancy and spice gradients on sub-measurement scales. Here, we assume that the buoyancy and spice gradients are anti-correlated at the scales that contribute to ϕ_d. In other words, we assume that $\left\langle\nabla b\cdot\nabla s_p\right\rangle = \left\langle\left|\nabla b\right|\left|\nabla s_p\right|\cos(\psi)\right\rangle \approx -\left\langle\left|\nabla b\right|\left|\nabla s_p\right|\right\rangle$, where

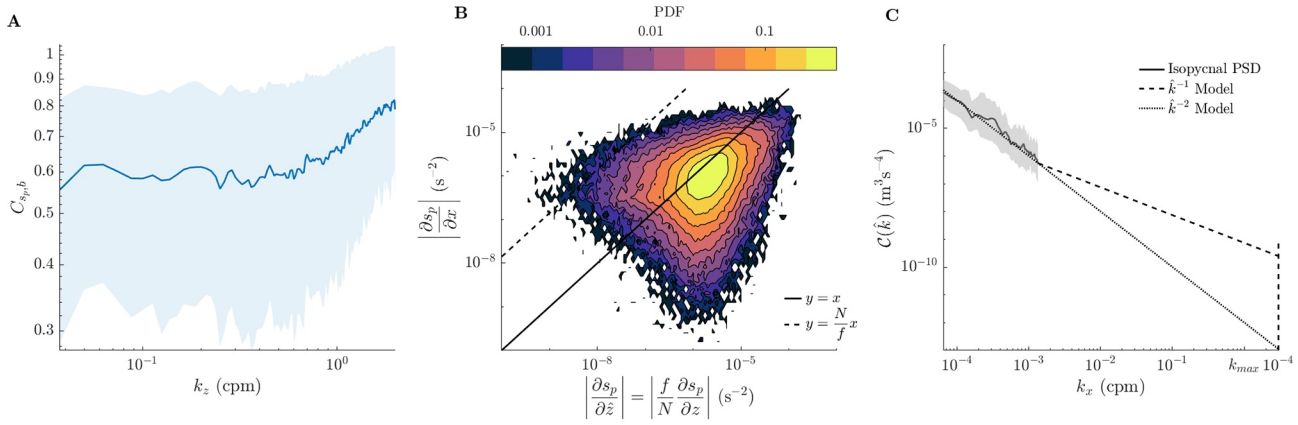

Figure 2. (a) Horizontal average of the magnitude-squared coherence of vertical gradients in spice and buoyancy calculated for each Conductivity, Temperature, Depth (CTD) cast plotted against stretched wavenumber $\tilde{k}_z = k_z \frac{f}{N}$. One standard deviation in shading. (b) PDF of spice gradients in stretched coordinates ($\tilde{z} = Nz/f$) on log scale. Lines correspond to isotropy in stretched coordinates ($y = x$) and unstretched coordinates ($y = Nx/f$). (c) PSD for spice variance along isopycnals, averaged with depth. Interquartile range of isopycnal spectra shown in shaded region.

$\cos(\psi)$ is the correlation coefficient. Since we assume that $\cos(\psi) = -1$, our method provides an approximate upper bound to the dissipation rate associated with double diffusion. There is evidence to support this assumptions in the data from Fine et al. (2018). Figure 2a shows the coherence between the vertical spice and buoyancy gradients

$$C_{s_p,b} = \frac{\overline{\left|\widehat{\partial_z s_p}\,\widehat{\partial_z b}^{*}\right|^2}}{\overline{\left|\widehat{\partial_z s_p}\right|^2}\;\overline{\left|\widehat{\partial_z b}\right|^2}}, \tag{3}$$

where $\hat{\cdot}$ denotes a Fourier transform applied to de-trended vertical profiles and $\bar{\cdot}$ refers to an average of different realizations of the spectrum. We calculate the coherence for each CTD cast, obtaining multiple realizations of the spectra using the method of Welch (1967). The line in Figure 2a shows the average of $C_{s_p,b}$ across all profiles with one standard deviation indicated by shading. The coherence increases at small scales, implying that buoyancy and spice gradients are correlated, so $\left\langle \left|\nabla b \cdot \nabla s_p\right| \right\rangle \approx -\left\langle \left|\nabla b\right| \left|\nabla s_p\right| \right\rangle$ is a reasonable assumption. While the coherence is positive by definition, the vertical buoyancy and spice gradients are anti-correlated when $|R_\rho| < 1$ which is true for most of the section (Figure 1c). Note that the averaging procedure does not heavily affect the sorted buoyancy gradient b_z^* by its definition.

When Equation 2 is evaluated directly with buoyancy and spice gradients calculated using the available observations, the corresponding dissipation rate is very small $\sim O(10^{-12})$ W/kg. This shows, unsurprisingly, that molecular diffusion is weak at the resolution of the observations (~300 m in the horizontal and ~0.5 m in the vertical). The central hypothesis of our method is that spice variance is transferred downscale by along-isopycnal stirring until it reaches a scale where the up-gradient buoyancy flux drives double-diffusive motions. Since the hypothesized stirring is along-isopycnal, we take the buoyancy gradient on sub-measurement scales to be constant. Specifically, this allows us to assume first that $\langle |\nabla b||\nabla s_p| \rangle \approx \langle |\nabla b| \rangle \langle |\nabla s_p| \rangle$, and second that $\langle |\nabla b| \rangle = |\langle \nabla b \rangle|$, so the buoyancy gradient magnitude can be estimated by the value on the measurement scale. However, we have not assumed that the spice gradient is constant on sub-measurement scales, so $\langle |\nabla s_p| \rangle \neq |\langle \nabla s_p \rangle|$ in general and we must estimate $\langle |\nabla s_p| \rangle$ by other means. In the next section we describe a method for estimating the magnitude of the spice gradient on sub-measurement scales.

3.2. Down-Scaled Spice Gradients

To estimate the sub-measurement-scale spice gradients, we use a statistical method based on the assumption that spice is stirred along isopycnals by quasi-geostrophic (QG) motions. The Rossby number

associated with the eddy shown in Figure 1 is about 0.2 which is not inconsistent with the QG limit (Fine et al., 2018). Based on theory from Charney (1971), Haynes and Anglade (1997) and Smith and Ferrari (2009) showed that QG flow generates filaments of passive tracers (such as spice) with a horizontal to vertical aspect ratio of N/f where N is the buoyancy frequency $N = \sqrt{-\partial b / \partial z}$ and f is the Coriolis parameter. The data appear to be generally consistent with an N/f aspect ratio. Lines with a slope matching the local f/N slope are indicated in panel a of Figure 1. Figure 2b shows a joint PDF of spice gradients in stretched coordinates. The peak in the distribution lies close to the $y = x$ line, corresponding to isotropy in the stretched coordinate system.

Based on QG theory, for scales that are small compared to the eddies responsible for stirring, spice variance is expected to follow $\tilde{k}^{-1}$ (inertial-convective scaling) where $\tilde{k} = \sqrt{k_x^2 + k_y^2 + \tilde{k}_z^2}$ is the wavenumber magnitude in the stretched coordinate system $(k_x, k_y, \tilde{k}_z) = (k_x, k_y, fk_z/N)$ (Smith & Ferrari, 2009). In contrast, the QG buoyancy variance spectrum is much steeper ($\sim \tilde{k}^{-5}$), consistent with our assumption that the buoyancy gradients are constant on sub-measurement scales. Based on this theory, we use the following model for the sub-measurement-scale spice power spectrum,

$$\mathcal{P}_{s_p}(\tilde{k}) = A\tilde{k}^{-1}, \tag{4}$$

where A is a pre-factor that depends on the rate of generation of spice variance. The dependence of Equation 4 on $\tilde{k}$ alone, reflects the isotropy of the spice variance in stretched coordinates. As will be discussed later, other forms of the spice variance spectrum can be used with this method.

The along-isopycnal spice variance spectrum from the Fine et al. (2018) data (Figure 2c) shows a $\tilde{k}^{-2}$ scaling, consistent with other observations of passive tracers at these scales (Callies & Ferrari, 2013; Klymak et al., 2015). Our modeled $\tilde{k}^{-1}$ spectrum at sub-measurement scales is indicated with a dashed line. MacKinnon et al. (2016) shows observational evidence for a k^{-1} scaling of temperature in salinity-controlled mixed layers for two separate observational datasets, however the transition to this scaling occurs at horizontal wavelengths ~300 m which is smaller than the available observations. In Section 4.1 we discuss the sensitivity of our results to the model spice power spectrum.

To estimate the spice gradients that contribute to ϕ_d we extrapolate the spice variance spectrum down to a scale corresponding to the convective overturns driven by double diffusion. Our underlying assumption is that the APE generated by the up-gradient buoyancy flux at this scale drives convective motions and that the resulting turbulence fluxes kinetic energy further downscale until it is dissipated at the same rate. Hence, although spice gradients will persist down to the haline Batchelor scale, we estimate the spice gradients at the scale of the largest 3d turbulent motions which we take to be the Ozmidov scale $L_{O_z} = \sqrt{\frac{\epsilon}{N^3}}$. This choice is consistent with the scaling for the layer thickness in diffusive convection proposed by Fernando (1989). Other choices are discussed in Zhou et al. (2016) who suggest that $L_Z = (\epsilon^3 / \kappa_T N^8)^{1/4}$ provides a better match with observations and lab experiments. However, since $L_{O_z} = (Re_b Pr)^{1/4} L_Z$ and Re_b is small for the Fine et al. (2018) data set (see Figure 3g) the two lengthscales yield similar dissipation rate estimates and we use L_{O_z} for simplicity.

We estimate the amplitude of the spice power spectrum, A, by calculating the along-isopycnal two-point correlation,

$$R(\tilde{r}) = \left\langle \mid s_p(\mathbf{x},t) - s_p(\mathbf{x} + \tilde{r}\mathbf{a},t) \mid^2 \right\rangle, \tag{5}$$

where $\tilde{r}$ is a distance in the stretched coordinate system and $\mathbf{a}$ is the along-isopycnal unit vector. Here, we calculate the two-point correlation between neighboring measurement points, interpolated vertically onto an isopycnal surface, centering our calculation of R between adjacent CTD casts. We can relate the two-point correlation to the spice power spectrum extrapolated down to the Ozmodiv scale by taking the Fourier transform of Equation 5 and applying the translation by $\tilde{r}\mathbf{a}$ as a wavenumber modulation in Fourier space, yielding

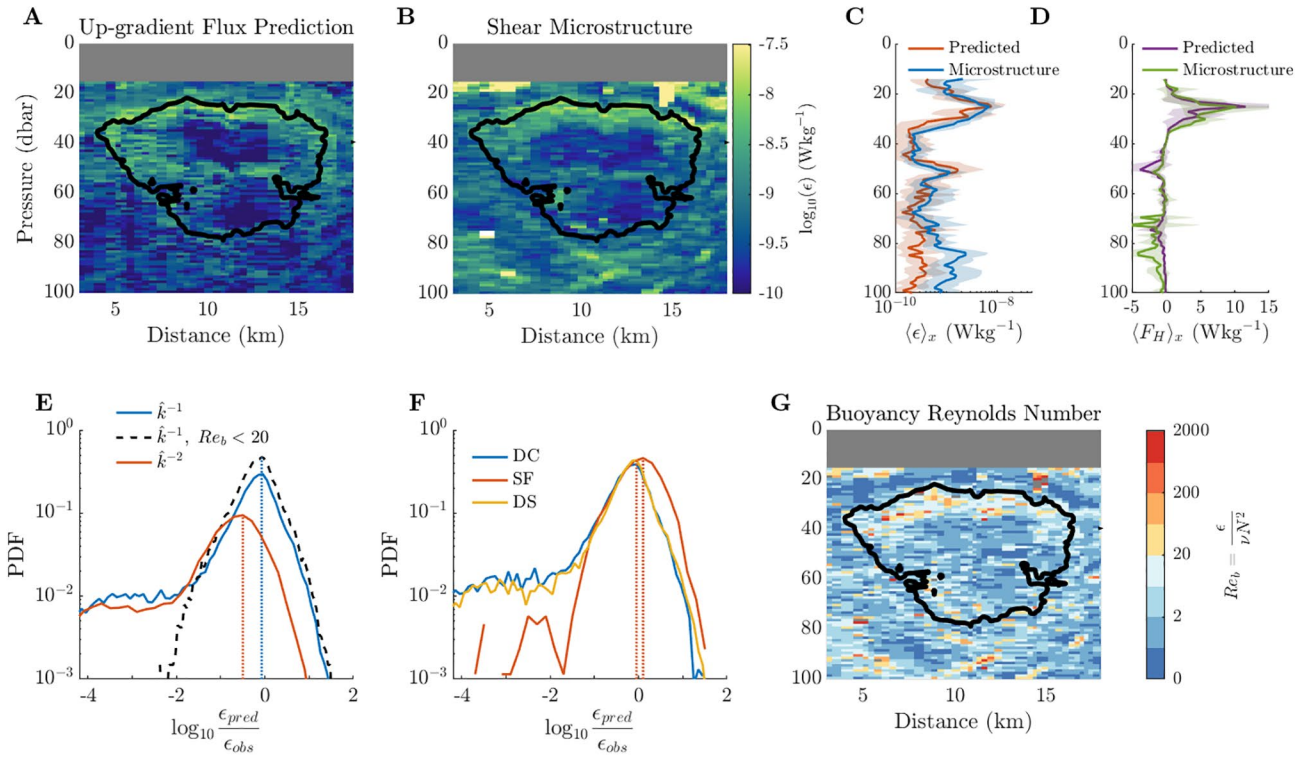

Figure 3. Comparison of predicted (a, b, and c) predicted dissipation rates ϵ (m^2s^{-3}) (a) with microstructure-inferred values (b) (Fine et al., 2018). (d), Osborn (1980) estimate for the heat flux using $\Gamma = 1$ for predicted and microstructure ϵ. Horizontal mean (c and d), taken between 8 and 13 km with shaded spatial standard deviations. (e and f) Log-histograms of ratio between the predicted ϵ_{pred} and observed ϵ_{obs} dissipation rate. (e) Data calculated using $\tilde{k}^{-1}$ model, $\tilde{k}^{-2}$ model and $\tilde{k}^{-1}$ model excluding points where $Re_b = \frac{\epsilon}{\nu N^2} > 20$. (f) Subdivision of data by $R_\rho = \alpha \frac{\partial T}{\partial z} \Big/ \beta \frac{\partial S}{\partial z}$ value (see text). (g) Buoyancy Reynolds number Re_b calculated using microstructure.

$$R(\tilde{r}) = 2\int_0^{\tilde{k}_{Oz}} \mathcal{P}_{s_p}(\tilde{k})(1 - \cos(\tilde{k}\tilde{r}))d\tilde{k}, \tag{6}$$

where $\tilde{k}_{Oz} = 2\pi f \,/\, (NL_{Oz})$ is the Ozmidov wavenumber in stretched coordinates. Using the model spice spectrum (Equation 4) then gives the amplitude

$$A = \frac{R(\tilde{r})}{2\int_0^{\tilde{k}_{Oz}} \tilde{k}^{-1}(1 - \cos(\tilde{r}\tilde{k}))d\tilde{k}}, \tag{7}$$

where the integral in the denominator is related to the exponential integral.

We can then estimate the spice gradient magnitude (in stretched coordinates) using the 2-norm $\left\langle \left|\tilde{\nabla} s_p\right| \right\rangle \approx \sqrt{\left\langle \left|\tilde{\nabla} s_p\right|^2 \right\rangle}$ and applying Parseval's theorem (in stretched coordinates), using the model spectrum from Equation 4,

$$\left\langle \left|\tilde{\nabla} s_p\right|^2 \right\rangle = \int_0^\infty \tilde{k}^2 \mathcal{P}_{s_p}(\tilde{k})\, d\tilde{k} = A\int_0^{\tilde{k}_{Oz}} \tilde{k} d\tilde{k} = \frac{1}{2} A \tilde{k}_{Oz}^2 \tag{8}$$

Applying isotropy in stretched coordinates, we can re-scale the vertical coordinate to write the average spice gradient in unstretched coordinates, $\langle |\nabla s_p| \rangle$, in terms of the spice gradient in stretched coordinates, $\left\langle \left|\tilde{\nabla} s_p\right| \right\rangle$, giving

$$\left\langle \left|\nabla s_p\right| \right\rangle = \sqrt{\frac{2}{3} + \frac{N^2}{3f^2}} \left\langle \left|\tilde{\nabla} s_p\right| \right\rangle. \quad (9)$$

Evaluating the spice gradient magnitude $|\nabla s_p|$ in Equation 2, we get the form for the average dissipation rate $\langle\epsilon\rangle$. In summary, the method can be written as a series of steps

Algorithm 1: Method summary

Step 1: Calculate the two-point correlation, $R(\vec{r})$, for the spice field (Eq. 5).
Step 2: Make an initial guess for $\langle\epsilon\rangle$ to estimate k_{Oz}.
Step 3: Calculate A using Eq. (7).
Step 4: Update the estimate for $\langle\epsilon\rangle$ using

$$\langle\epsilon\rangle = -\langle\phi_d\rangle = -\frac{\kappa_T + \kappa_S}{2b_z^*}\langle|\nabla b|^2\rangle + g\frac{\kappa_T - \kappa_S}{2b_z^*}\langle|\nabla b|\rangle\sqrt{\frac{2}{3} + \frac{N^2}{3f^2}}\sqrt{\frac{A}{2}}k_{Oz}, \quad (10)$$

applied at each point.
Step 5: Return to Step 3 and continue until $\langle\epsilon\rangle$ converges.

4. Results

4.1. Comparison With Microstructure

The result of our method as applied to the data from Fine et al. (2018) are shown in Figure 3a. The match between the estimated and measured dissipation rates is generally very good. Both the pattern and magnitude of the dissipation are captured by the method, even in areas of doubly stable stratification, not traditionally thought of as active areas of double-diffusive convection. In the centre of the eddy, where the stratification is very weak, the method predicts very low levels of dissipation ($<10^{-10}$ m^{2}s^{-3}), however the noise floor for the shear probe observations of ϵ is about 10^{-10} m^{2}s^{-3} so we cannot compare these small values. Comparing the horizontal averages of dissipation rate on the right we can also see the close match between observations and our method. Figure 3d shows the horizontal average of the heat flux inferred from the dissipation rate using the Osborn (1980) method using a mixing efficiency $\Gamma = 1$, following Fine et al. (2018) and St. Laurent and Schmitt (1999). Following the method described in Fine et al. (2018) we exclude values where 'interfaces' were identified using a threshold $\frac{\partial T}{\partial z} > 0.2$ °Cm^{-1}). The agreement between the Osborn (1980) method for microstructure and our prediction implies that we can also estimate heat fluxes along the top and sides of the eddy. There is a discrepancy beneath the eddy that is discussed below, which suggests that double diffusion is not the dominate source of turbulence in this region.

Microstructure measurements of ϵ have an uncertainty of a factor of around 2 (Fine et al., 2018). Histograms of the ratio of the estimated and observed dissipation rates are shown in Figure 3e and 3f (points with ϵ_{pred} below the instrument noise floor of 10^{-10} m^{2}s^{-3} are excluded). The comparison in panel e shows a log-normal distribution around an average bias of 0.89 with a tail to the distribution for small values. The mean bias corresponds to an average observed dissipation of 9.7×10^{-10} m^{2}s^{-3} and average predicted dissipation of 8.5×10^{-10}m^{2}s^{-3}. Excluding points with buoyancy Reynolds numbers $Re_b = \frac{\epsilon}{\nu N^2} > 20$ (a threshold value for double-diffusion used by Inoue et al. (2007) amongst others) removes the tail such that 72% of the estimated dissipation rates are within a factor of 3 of the observed values, although note that very little data here has $Re_b > 20$ (as shown in Figure 3g). Differences between our prediction and observations (at low Re_b) are similar to those occurring due to natural variability (Moum et al., 1995). The enhanced Re_b may be the result of shear as the Richardson number is smaller above and below the eddy (Figure 1), however it is still unclear when shear will damp or enhance double-diffusive convection (Padman, 1994; Shibley & Timmermans, 2019). The enhanced Re_b beneath the eddy explains the discrepancy between the horizontally averaged prediction and observation in Figure 3c.

Panel f divides the data between areas usually identified as 'double-diffusive convection favorable' ($0 < R_\rho < 1$), 'salt fingering favorable' ($R_\rho > 1$) and 'doubly-stable' ($R_\rho < 0$). This panel shows that the method works well for 'DC' and 'DS' regimes but potentially overestimates the dissipation rate in 'SF' regimes. It is possible that salt-fingers are present, which may change the appropriate overturning length scale. Another explanation is that our assumption of anti-correlating buoyancy and spice gradients breaks down for

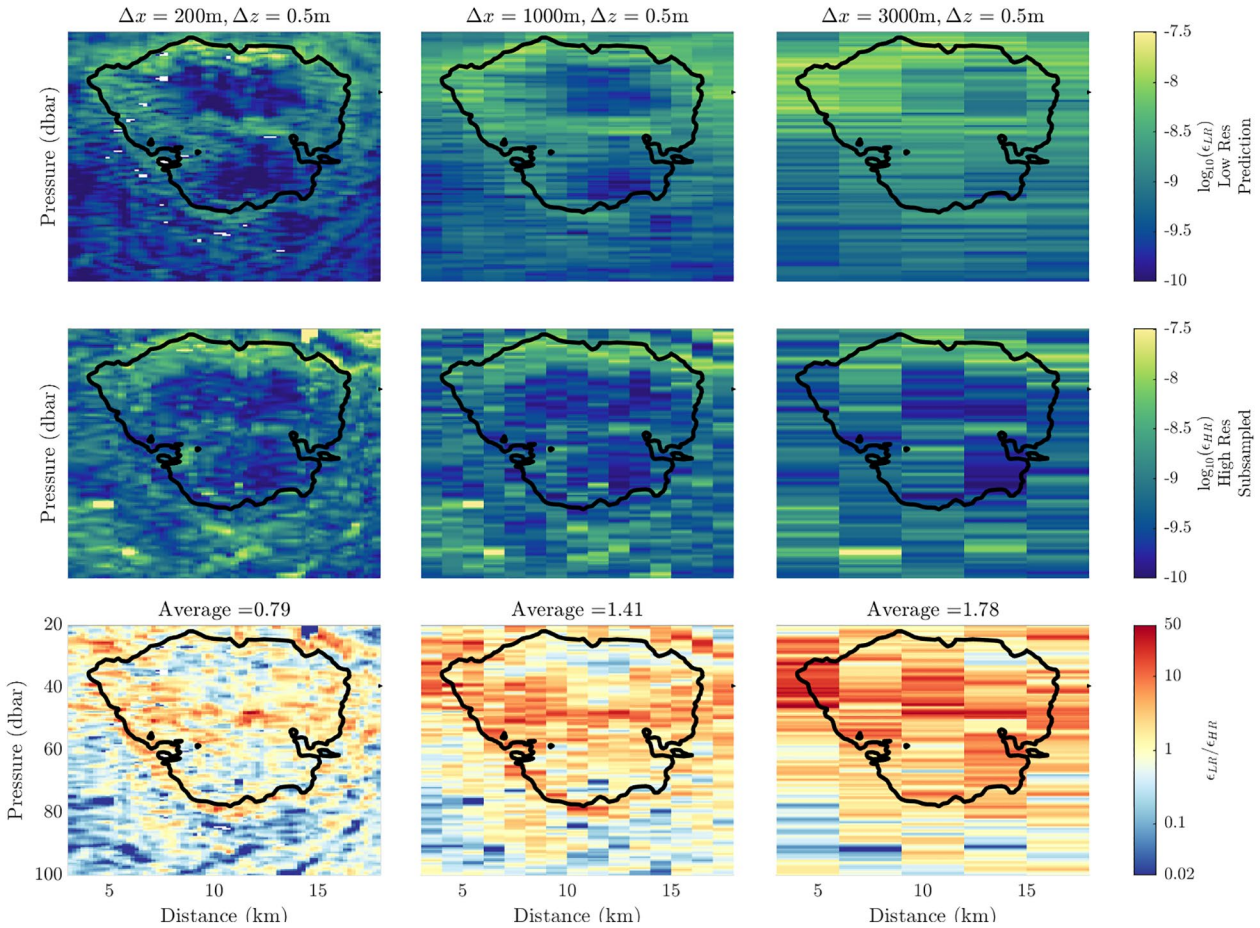

Figure 4. Top row shows inferred dissipation rate ϵ using T/S data sampled at the given resolution in the title. Middle row shows observed ϵ using full T/S data, subsampled at the given resolution. Bottom row shows ratio between top and middle figure values. Colorbar is on a log-scale and mean value corresponds to the peak of the distribution of $\epsilon_{pred}/\epsilon_{obs}$.

$|R_\rho| > 1$. However, there is too little 'SF'-data here to fully analyze these possibilities and the method still works relatively well in 'SF' regions. Alternatively, if we were to assume a persistent $\tilde{k}^{-2}$ scaling down to the Ozmidov scale, the patterns of the estimated dissipation rate would be qualitatively similar, but the magnitude of the dissipation rate would decrease by about a factor of 3 (see panel e). The model spice spectrum represents the largest sensitivity in the method and further observations of the $\mathcal{O}(1) - \mathcal{O}(100)$ m scales could help test and improve the method.

4.2. Method Sensitivity

The T/S section from Fine et al. (2018) has a high resolution ($\Delta x \sim$ 200–1000 m in the horizontal and $\Delta z = 0.25$ m in the vertical). A natural question is whether the method would work when applied to a lower resolution section of T/S. To test this, we sub-sample the original data at lower horizontal resolution. Figure 4 shows three different resolution comparisons in the three columns. In each comparison we calculate the dissipation rate using subsampled temperature and salinity sections, and we compare the result with the observed double-diffusive dissipation rate subsampled at the same resolution. Note that the data in Figure 4 are calculated based on horizontally gridded T/S data, whereas the method in Figure 3a is applied to ungridded data (which gives a better agreement with observations). Using lower resolution T/S data somewhat increases the estimated dissipation rate, although the method performs well even at significantly reduced resolution. This suggests that our method could be applied to lower resolution CTD sections which are much more widely available.

For the observations of Fine et al. (2018), the first term in Equation 10 is small, and $N \gg f$, so we can write

$$\langle \epsilon \rangle = \left(\frac{1}{\sqrt{6}} \pi g (\kappa_T - \kappa_S) \frac{\langle |\nabla b| \rangle}{b_z^*} N^{\frac{3}{2}} \sqrt{A} \right)^{\frac{2}{3}}. \quad (11)$$

Equation 11 more clearly shows the dependence of $\langle \epsilon \rangle$ on the rate of generation of spice variance via A, the buoyancy frequency N and the term $\langle |\nabla b| \rangle / b_z^*$ which gives a measure of the curvature of isopycnals. If we set the term $\langle |\nabla b| \rangle / b_z^*$ constant, we underestimate the dissipation rate along the top of the eddy, where the isopycnals heave, suggesting that the large-scale variations in density may have a direct effect on the small scale turbulence.

If we vary the spice spectrum amplitude A (Equation 7), by a scale factor a, although the pattern of the dissipation rate remains similar to Figure 3a, the magnitude changes by a factor of about $a^{1/3}$ (by considering Equation 11). Therefore, an error in A by a factor of 10 would result in an estimate of ϵ that is incorrect by a factor of ~2.15. This relatively low sensitivity to A is the reason for the lack of sensitivity to the scale at which the $\tilde{k}^{-2}$ spectrum transitions to $\tilde{k}^{-1}$ in our model. This also explains why the method maintains skill at low resolution (Figure 4) despite the disagreement between the assumed $\tilde{k}^{-1}$ spectrum and the observed $\tilde{k}^{-2}$ spectrum (Figure 2). This effect may be corrected for by using a more complex model spectrum, however that is left as future work. The size of the eddy is also important here. The $\tilde{k}^{-1}$ slope is hypothesized to be the result of the eddy stirring, so for larger eddies we may expect the $\tilde{k}^{-1}$ model spectrum to hold at larger scales.

Although we calculate α and β at each grid point using the fully nonlinear equation of state, we assume a linear equation of state on sub-measurement scales in our method. If we use a single constant value for α and β across the whole section, the estimated dissipation rate would change by up to a factor of 1.8, so the effects of a nonlinear equation of state also represent an uncertainty in our method that may explain some of the discrepancies in Figure 4.

5. Conclusion

We have introduced a new method for estimating the dissipation rates associated with double diffusive turbulence from a temperature and salinity section. We used an energetic argument and a statistical approach which applies to general double-diffusive processes. For points with low buoyancy Reynolds number ($Re_b < 20$) in the data from Fine et al. (2018), our method closely matches observations (72% of estimated dissipation rates are within the observational uncertainty). Fine et al. (2018) used observations of dissipation rate to infer heat fluxes that matched those calculated using thermal microstructure observations. The close match in dissipation rates between our method and observations suggests our method may be used to infer heat fluxes in other locations where double diffusion is active. Finally, we showed that our method can be applied (with additional uncertainties) to T/S data with coarse spatial resolution, opening the door to applying the method to more widely-available lower resolution CTD sections.

Data Availability Statement

Shipboard and microstructure data are available for download (http://www.rvdata.us/catalog/SKQ201511S and https://microstructure.ucsd.edu, respectively). Code for applying our method to CTD data can be found at https://doi.org/10.5281/zenodo.4665777.

Acknowledgments
The authors thank Barry Ruddick and an anonymous reviewer for their valuable input on the development of this manuscript. This work was supported by the Natural Environment Research Council (grant number NE/L002507/1).

References

Bebieva, Y., & Timmermans, M.-L. (2016). An examination of double-diffusive processes in a mesoscale eddy in the Arctic Ocean. *Journal of Geophysical Research: Oceans*, *121*, 457–475. https://doi.org/10.1002/2015jc011105

Bebieva, Y., & Timmermans, M.-L. (2019). Double-diffusive layering in the Canada basin: An explanation of along-layer temperature and salinity gradients. *Journal of Geophysical Research: Oceans*, *124*, 723–735. https://doi.org/10.1029/2018jc014368

Callies, J., & Ferrari, R. (2013). Interpreting energy and tracer spectra of upper-ocean turbulence in the submesoscale range (1–200 km). *Journal of Physical Oceanography*, *43*(11), 2456–2474. https://doi.org/10.1175/jpo-d-13-063.1

Carmack, E., Polyakov, I., Padman, L., Hunke, E., Hutchings, J., Hutchings, J., et al. (2015). Toward quantifying the increasing role of oceanic heat in sea ice loss in the new Arctic. *Bulletin of the American Meteorological Society*, *96*(12), 2079–2105. https://doi.org/10.1175/bams-d-13-00177.1

Carmack, E. C., Williams, W. J., Zimmermann, S. L., & McLaughlin, F. A. (2012). The Arctic Ocean warms from below. *Geophysical Research Letters*, *39*, L07604. https://doi.org/10.1029/2012gl050890

Charney, J. G. (1971). Geostrophic turbulence. *Journal of the Atmospheric Sciences*, *28*(6), 1087–1095. https://doi.org/10.1175/1520-0469(1971)028<1087:gt>2.0.co;2

Fernando, H. J. (1989). Oceanographic implications of laboratory experiments on diffusive interfaces. *Journal of Physical Oceanography*, *19*(11), 1707–1715. https://doi.org/10.1175/1520-0485(1989)019<1707:oioleo>2.0.co;2

Fine, E. C., MacKinnon, J. A., Alford, M. H., & Mickett, J. B. (2018). Microstructure observations of turbulent heat fluxes in a warm-core Canada basin eddy. *Journal of Physical Oceanography*, *48*(10), 2397–2418. https://doi.org/10.1175/jpo-d-18-0028.1

Garrett, C. (1982). On the parameterization of diapycnal fluxes due to double-diffusive intrusions. *Journal of Physical Oceanography*, *12*(9), 952–959. https://doi.org/10.1175/1520-0485(1982)012<0952:otpodf>2.0.co;2

Gregg, M. (1989). Scaling turbulent dissipation in the thermocline. *Journal of Geophysical Research*, *94*(C7), 9686–9698. https://doi.org/10.1029/jc094ic07p09686

Gregg, M., D'Asaro, E., Riley, J., & Kunze, E. (2018). Mixing efficiency in the ocean. *Annual Review of Marine Science*, *10*, 443–473. https://doi.org/10.1146/annurev-marine-121916-063643

Haynes, P., & Anglade, J. (1997). The vertical-scale cascade in atmospheric tracers due to large-scale differential advection. *Journal of the Atmospheric Sciences*, *54*(9), 1121–1136. https://doi.org/10.1175/1520-0469(1997)054<1121:tvscia>2.0.co;2

Holleman, R., Geyer, W., & Ralston, D. (2016). Stratified turbulence and mixing efficiency in a salt wedge estuary. *Journal of Physical Oceanography*, *46*(6), 1769–1783. https://doi.org/10.1175/jpo-d-15-0193.1

Howland, C. J., Taylor, J. R., & Caulfield, C. (2020). Mixing in forced stratified turbulence and its dependence on large-scale forcing. *Journal of Fluid Mechanics*, 898.

Inoue, R., Yamazaki, H., Wolk, F., Kono, T., & Yoshida, J. (2007). An estimation of buoyancy flux for a mixture of turbulence and double diffusion. *Journal of Physical Oceanography*, *37*(3), 611–624. https://doi.org/10.1175/jpo2996.1

Jackett, D. R., & McDougall, T. J. (1985). An oceanographic variable for the characterization of intrusions and water masses. *Deep Sea Research Part A. Oceanographic Research Papers*, *32*(10), 1195–1207. https://doi.org/10.1016/0198-0149(85)90003-2

Jackson, P. R., & Rehmann, C. R. (2003). Laboratory measurements of differential diffusion in a diffusively stable, turbulent flow. *Journal of Physical Oceanography*, *33*(8), 1592–1603. https://doi.org/10.1175/2405.1

Klymak, J. M., Crawford, W., Alford, M. H., MacKinnon, J. A., & Pinkel, R. (2015). Along-isopycnal variability of spice in the north pacific. *Journal of Geophysical Research: Oceans*, *120*, 2287–2307. https://doi.org/10.1002/2013jc009421

Kunze, E. (2003). A review of oceanic salt-fingering theory. *Progress in Oceanography*, *56*(3–4), 399–417. https://doi.org/10.1016/s0079-6611(03)00027-2

MacKinnon, J. A., Nash, J. D., Alford, M. H., Lucas, A. J., Mickett, J. B., Shroyer, E. L., et al. (2016). A tale of two spicy seas. *Oceanography*, *29*(2), 50–61. https://doi.org/10.5670/oceanog.2016.38

Middleton, L., & Taylor, J. R. (2020). A general criterion for the release of background potential energy through double diffusion. *Journal of Fluid Mechanics*, 893.

Moum, J., Gregg, M., Lien, R., & Carr, M. (1995). Comparison of turbulence kinetic energy dissipation rate estimates from two ocean microstructure profilers. *Journal of Atmospheric and Oceanic Technology*, *12*(2), 346–366. https://doi.org/10.1175/1520-0426(1995)012<0346:cotked>2.0.co;2

Osborn, T. R. (1980). Estimates of the local rate of vertical diffusion from dissipation measurements. *Journal of Physical Oceanography*, *10*(1), 83–89. https://doi.org/10.1175/1520-0485(1980)010<0083:eotlro>2.0.co;2

Osborn, T. R., & Cox, C. S. (1972). Oceanic fine structure. *Geophysical Fluid Dynamics*, *3*(4), 321–345. https://doi.org/10.1080/03091927208236085

Padman, L. (1994). Momentum fluxes through sheared oceanic thermohaline steps. *Journal of Geophysical Research*, *99*(C11), 22491–22499. https://doi.org/10.1029/94jc01741

Polzin, K. L., Garabato, A. C. N., Huussen, T. N., Sloyan, B. M., & Waterman, S. (2014). Finescale parameterizations of turbulent dissipation. *Journal of Geophysical Research: Oceans*, *119*, 1383–1419. https://doi.org/10.1002/2013jc008979

Ruddick, B., & Kerr, O. (2003). Oceanic thermohaline intrusions: Theory. *Progress in Oceanography*, *56*(3–4), 483–497. https://doi.org/10.1016/s0079-6611(03)00029-6

Ruddick, B., & Richards, K. (2003). Oceanic thermohaline intrusions: Observations. *Progress in Oceanography*, *56*(3–4), 499–527. https://doi.org/10.1016/s0079-6611(03)00028-4

Rudnick, D. L., & Ferrari, R. (1999). Compensation of horizontal temperature and salinity gradients in the ocean mixed layer. *Science*, *283*(5401), 526–529. https://doi.org/10.1126/science.283.5401.526

Schmitt, R. W. (1994). Double diffusion in oceanography. *Annual Review of Fluid Mechanics*, *26*(1), 255–285. https://doi.org/10.1146/annurev.fl.26.010194.001351

Shibley, N., & Timmermans, M.-L. (2019). The formation of double-diffusive layers in a weakly turbulent environment. *Journal of Geophysical Research: Oceans*, *124*, 1445–1458. https://doi.org/10.1029/2018jc014625

Shibley, N., Timmermans, M.-L., Carpenter, J., & Toole, J. (2017). Spatial variability of the Arctic Ocean's double-diffusive staircase. *Journal of Geophysical Research: Oceans*, *122*, 980–994. https://doi.org/10.1002/2016jc012419

Shimada, K., Kamoshida, T., Itoh, M., Nishino, S., Carmack, E., McLaughlin, F., & Proshutinsky, A. (2006). Pacific Ocean inflow: Influence on catastrophic reduction of sea ice cover in the Arctic Ocean. *Geophysical Research Letters*, *33*, L08605. https://doi.org/10.1029/2005gl025624

Smith, K. S., & Ferrari, R. (2009). The production and dissipation of compensated thermohaline variance by mesoscale stirring. *Journal of Physical Oceanography*, *39*(10), 2477–2501. https://doi.org/10.1175/2009jpo4103.1

St Laurent, L., & Schmitt, R. W. (1999). The contribution of salt fingers to vertical mixing in the north Atlantic tracer release experiment. *Journal of Physical Oceanography*, *29*(7), 1404–1424. https://doi.org/10.1175/1520-0485(1999)029<1404:tcosft>2.0.co;2

Timmermans, M.-L., & Marshall, J. (2020). Understanding Arctic Ocean circulation: A review of ocean dynamics in a changing climate. *Journal of Geophysical Research: Oceans*, *125*, e2018JC014378. https://doi.org/10.1029/2018jc014378

Timmermans, M.-L., Toole, J., & Krishfield, R. (2018). Warming of the interior arctic ocean linked to sea ice losses at the basin margins. *Science Advances*, *4*(8), eaat6773. https://doi.org/10.1126/sciadv.aat6773

Timmermans, M.-L., Toole, J., Krishfield, R., & Winsor, P. (2008). Ice-tethered profiler observations of the double-diffusive staircase in the Canada basin thermocline. *Journal of Geophysical Research*, *113*, C00A02. https://doi.org/10.1029/2008jc004829

Watanabe, E. (2011). Beaufort shelf break eddies and shelf-basin exchange of pacific summer water in the western Arctic Ocean detected by satellite and modeling analyses. *Journal of Geophysical Research*, *116*, C08034. https://doi.org/10.1029/2010jc006259

Welch, P. (1967). The use of fast Fourier transform for the estimation of power spectra: A method based on time averaging over short, modified periodograms. *IEEE Transactions on Audio and Electroacoustics*, *15*(2), 70–73. https://doi.org/10.1109/tau.1967.1161901

Whalen, C. B., MacKinnon, J. A., Talley, L. D., & Waterhouse, A. F. (2015). Estimating the mean diapycnal mixing using a finescale strain parameterization. *Journal of Physical Oceanography*, *45*(4), 1174–1188. https://doi.org/10.1175/jpo-d-14-0167.1

Winters, K. B., Lombard, P. N., Riley, J. J., & D'Asaro, E. A. (1995). Available potential energy and mixing in density-stratified fluids. *Journal of Fluid Mechanics*, *289*, 115–128. https://doi.org/10.1017/s00221120950012 5x

Zhou, S.-Q., Lu, Y.-Z., Song, X.-L., & Fer, I. (2016). New layer thickness parameterization of diffusive convection in the ocean. *Dynamics of Atmospheres and Oceans*, *73*, 87–97. https://doi.org/10.1016/j.dynatmoce.2016.01.001